International Scholarly Research Network
ISRN Nanomaterials
Volume 2012, Article ID 865373, 8 pages
doi:10.5402/2012/865373

*Research Article*

# Synthesis and Optical Characterization of $Mg_{1-x}Ni_xO$ Nanostructures

**Nageswararao Budiredla,[1] Ashok Kumar,[1,2] Subhash Thota,[3] and Jitendra Kumar[1]**

[1] *Materials Science Programme, Indian Institute of Technology Kanpur, Kanpur 208016, India*
[2] *Bio-Inspired Materials and Devices Laboratory (BMDL), Center for Energy Harvesting Materials and Systems (CEHMS), Virginia Tech, Blacksburg, VA 24061, USA*
[3] *Department of Physics, Indian Institute of Technology Guwahati, Guwahati 781039, India*

Correspondence should be addressed to Jitendra Kumar, jk@iitk.ac.in

Received 23 September 2012; Accepted 11 October 2012

Academic Editors: C. Angeles-Chavez, B. A. Marinkovic, and B. Panchapakesan



An attempt has been made here to synthesize $Mg_{1-x}Ni_xO$ ($0.01 \leq x \leq 0.10$) nano-powders via sol-gel process. These powders are shown to possess an f.c.c. (NaCl-type) structure with a typical lattice parameter of 4.228(2) Å for "$x$" = 0.01 when decomposition of dried oxalate gel product is carried out at 600°C for 2 h in air. Moreover, they exhibit (i) clusters/agglomerates of nanosize particles and (ii) high BET specific surface area (123.0–135.5 $m^2/g$). Also, the infrared absorption spectra reveal their strong affinity to water. The UV-Vis absorption peaks appearing at ~202 nm, 296 nm, and 379 nm are associated with oxygen defect centres and correspond to the electronic transitions (i) $^1A_{1g} \rightarrow {}^1T_{1u}$ ($1s \rightarrow 2p_x$, $2p_y$, or $2p_z$), (ii) $^1A_{1g} \rightarrow {}^1E$ ($1s \rightarrow 2p_x$, or $2p_y$) and (iii) $^1A_{1g} \rightarrow {}^1A_{1g}$ ($1s \rightarrow 2p_z$), respectively. The incorporation of $Ni^{2+}$ ions causes some modifications in the energy levels and the optical absorbance characteristics. The suppression of a strong broad emission peak at 440 nm and improvement of a weak band at ~400 nm in the photoluminescence (PL) spectrum arise due to decrease in population density of $F_2{}^{2+}$ centres (or $F^+$ dimmers) and emergence of additional $F^+$centres, respectively with increase in nickel content.

## 1. Introduction

Magnesium oxide (MgO) exhibits an f.c.c. (NaCl-type) crystal structure, high thermal stability, predominantly ionic nature, and insulating behaviour [1]. MgO has been extensively used in catalysis, toxic waste remediation, antibacterial materials, refractories, paints, and superconductors due to its unique optical, electronic, magnetic, thermal, mechanical, and chemical properties [2–8]. Recently, it has found promising application in plasma display panels [9]. Of particular interest is MgO nanopowder because of inherent size effects, for example, large surface area-to-volume ratio [10]. Various investigations have been undertaken earlier on its optical and electrical properties [2, 8, 11]. Surface anions with low coordination, considered to be chemically active sites, form excitons and give rise to specific optical transitions in the UV range [5, 8]. The processes usually used to synthesize MgO nanopowders include thermal evaporation, flame spray pyrolysis, laser vaporization, chemical gas phase deposition, combustion, aqueous wet chemical, vapor-phase transport, sol-gel, and hydrothermal reaction [5, 8, 12–15].

The incorporation of another element into a parent phase (i.e., oxide matrix) leads to crystal defects (e.g., vacancies, interstitials, and antisites) which, in turn, can modify the useful characteristics [16, 17]. Recently, interest arose in transition metal and rare earth-doped oxides mainly due to their excellent luminescence efficiency and application in lasers, optical amplifiers, and plasma display panels [18–21]. In transition metal ions, the d–d absorptions are parity forbidden and therefore charge carriers get excited mainly from the host oxide. In such a situation, absorption can be improved by enhancing the energy transfer from host to doped transition metal ions and/or reducing the influence of defects. Also, the addition of coactive ions or charge compensators (e.g., silicon or nickel) sometime facilitates absorption process resulting in the enhancement of the

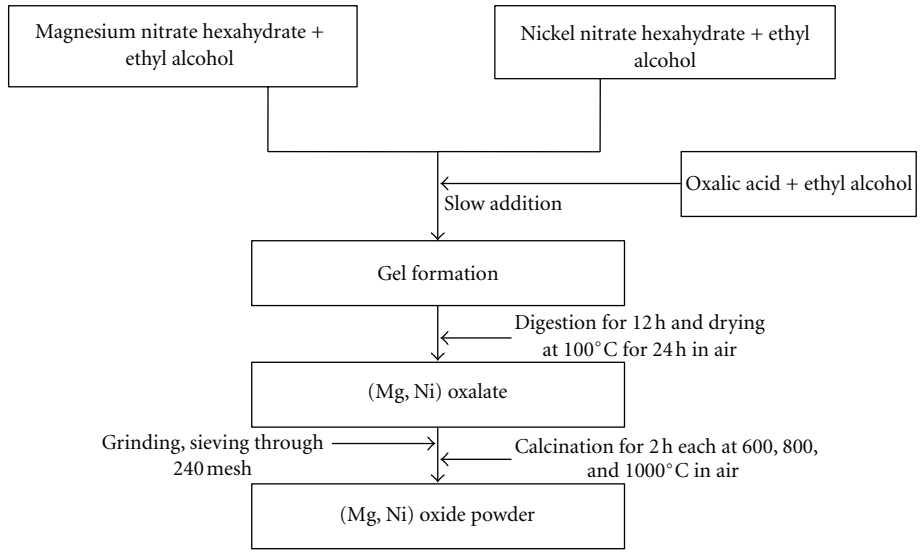


Scheme 1: Flow chart of the synthesis process of nickel doped magnesium oxide.

luminescence intensity [20, 21]. Nickel is a well-known activator for many inorganic systems and produces white light by suitably adjusting the yellow and blue light emissions [20, 21].

An attempt has been made here to study the effect of nickel doping on the crystal structure, morphology, particle size, optical absorption, and photoluminescence (PL) behaviour of MgO nanopowder with the objective of its possible application in optical devices. Sol-gel process has been chosen for synthesis because of its distinct advantage of being simple, cost effective, low processing temperature, high purity, and chemical homogeneity [22, 23].

## 2. Experimental Details

For synthesis, magnesium nitrate hexahydrate [$Mg(NO_3)_2 \cdot 6H_2O$], nickel nitrate hexahydrate [$Ni(NO_3)_2 \cdot 6H_2O$], and oxalic acid [$C_2H_2O_4 \cdot 2H_2O$] were used as precursors with ethanol as a solvent. First, 20 g of magnesium nitrate hexahydrate was added slowly to 200 mL of ethyl alcohol and stirred at 25°C until complete dissolution. Second, an appropriate amount of nickel nitrate hexahydrate was dissolved in 100 mL of ethyl alcohol similarly. Both these solutions were then mixed and oxalic acid solution (prepared in 200 mL of alcohol by taking metal to oxalate ion ratio as 1 : 1) added slowly with constant stirring to produce a thick white gel. The product was subsequently digested for 12 h, dried at 100°C for 24 h to yield presumably Ni-doped magnesium oxalate dihydrate which, in turn, was decomposed for 2 h each at 600, 800, and 1000°C to obtain $Mg_{1-x}Ni_xO$ ($0.01 \leq x \leq 0.10$) powder. The flow chart of synthesis process is given in Scheme 1.

To ascertain the condition of oxide formation, use was made of a thermogravimetry (TG) setup in the temperature range of 100–700°C. X-ray diffraction (XRD) patterns of various powder products were recorded with a diffractometer (Thermo Electron model ARL X'TRA) using the Cu $K\alpha_1$ radiation (wavelength = 1.54062 Å) and used for identification of phase(s) and evaluation of the average grain size. The morphology was observed in a scanning electron microscope (FEI Model Quanta 200 HV SEM) using a secondary electron (SE) mode. For this, the powder was dispersed over a copper stub and coated with the gold film to avoid charging and improve the SE signal. Pore-size distribution and BET surface area data were deduced from nitrogen adsorption-desorption isotherms recorded with a gas adsorption analyzer (Micromeritics model ASPS-2400). Prior to the physisorption, the samples were heated at 120°C for 30 min in nitrogen atmosphere. A Fourier transform infrared (FTIR) spectrometer (BRUKER Vertex-70) was used for detection of hydroxyl (−OH) and other groups in oxalates and –OH– stretching mode in oxide samples. For optical absorption measurements, a double beam UV-VIS-NIR spectrophotometer (Varian Cary 5000) was employed in the wavelength range of 200–800 nm. Further, the photoluminescence (PL) spectra were obtained with a Spex Fluorolog II Spectrophotometer at the excitation wavelength of 350 nm.

## 3. Results and Discussion

*3.1. Formation of Nickel Containing MgO.* Thermogravimetric analysis (TGA) of the sol-gel product was undertaken to gather information about its thermal stability and the formation of nickel containing MgO powders. For this, weight of sol-gel product (initially, 0.384 g) has been monitored by raising its temperature at a rate of 4°C/min from 100 to 700°C in air. Figure 1 shows the weight percentage ($W\%$) and derivative ($-dW\%/dT$) versus temperature plots of sample containing Ni/(Ni+Mg) atomic ratio of 0.01, dried at 100°C for 24 h. Accordingly, the first weight loss of ~22.5% occurs in the temperature range of 160–244°C with peak at 218°C. This weight loss can be attributed to removal of crystallizing water of presumably mixed oxalate

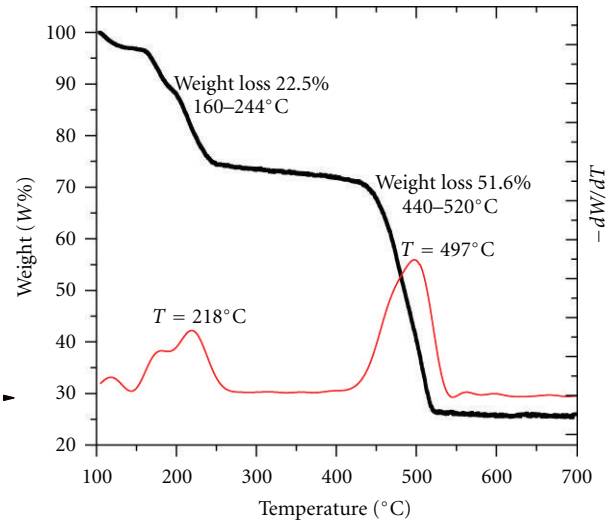


Figure 1: Percentage weight ($W\%$) versus temperature ($T$) and ($-dW\%/dT$) versus $T$ plots of dried sol-gel product containing [Ni/(Ni+Mg)] atomic ratio of 0.01.

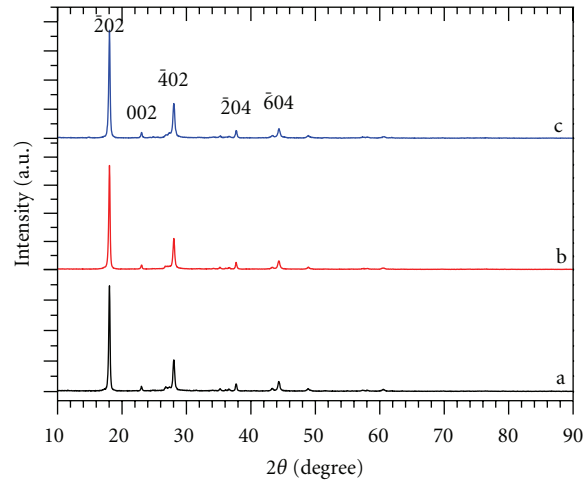


Figure 2: XRD patterns of the sol-gel products dried at 100°C for 24 h showing emergence of a monoclinic phase, similar to $\alpha$ – MgC2O4 · $2H_2O$, for [Ni/(Ni+Mg)] atomic ratio (a) 0.01, (b) 0.05, and (c) 0.10.

(Mg, Ni) $C_2O_4 \cdot 2H_2O$, which is 24.4 wt% and follow the reaction

$$(\mathrm{Mg,Ni})\mathrm{C_2O_4 \cdot 2H_2O} \longrightarrow (\mathrm{Mg,Ni})\mathrm{C_2O_4} + 2\mathrm{H_2O}\,(\uparrow). \quad (1)$$

In the second stage, the weight loss of 51.6 wt% observed in the temperature range of 440–520°C (peak at 497°C) matches reasonably well with the evolution of CO and $CO_2$ (amounting to ~48.9%) from the anhydrous oxalate, (Mg, Ni) $C_2O_4$. The overall reaction can be written as

$$(\mathrm{Mg,Ni})\mathrm{C_2O_4} \xrightarrow{440-520^\circ\mathrm{C}} (\mathrm{Mg,Ni})\,\mathrm{O} + \mathrm{CO}\,(\uparrow) + \mathrm{CO_2}\,(\uparrow). \quad (2)$$

The slight discrepancy in weight loss can be understood if removal of water is partial in the first stage and the remaining amount gets evolved later in the temperature range of 440–520°C. No apparent weight change (i.e., loss or gain) occurs beyond 520°C. The final product reduced to about 26% of the initial weight. Accordingly, the decomposition temperature of 600°C or above can be chosen for the formation of a stable compound.

X-ray diffraction (XRD) patterns of the sol-gel products dried at 100°C for 24 h are shown in Figure 2. Their analysis suggests the emergence of a phase similar to magnesium oxalate dihydrate [$\alpha$-$MgC_2O_4 \cdot 2H_2O$] having monoclinic structure with lattice parameters $a = 12.68$ Å, $b = 5.391$ Å, $c = 9.977$ Å, $\beta = 129.82$, and $Z = 4$ [JCPDS # 26-1223]. Further, there is no evidence to indicate the presence of nickel or nickel compound in the product. Figure 3 shows XRD patterns of $Mg_{1-x}Ni_xO$ ($x = 0.01, 0.05$, and 0.10) powders obtained by decomposition of respective dried sol-gel oxalate for 2 h each at 600°C. These patterns are similar in nature and correspond to f.c.c. (NaCl-type) structure of MgO [JCPDS # 45-0946] with marginal variation in the lattice parameter, typical value being 4.228 ± 0.002 Å for powder with nickel

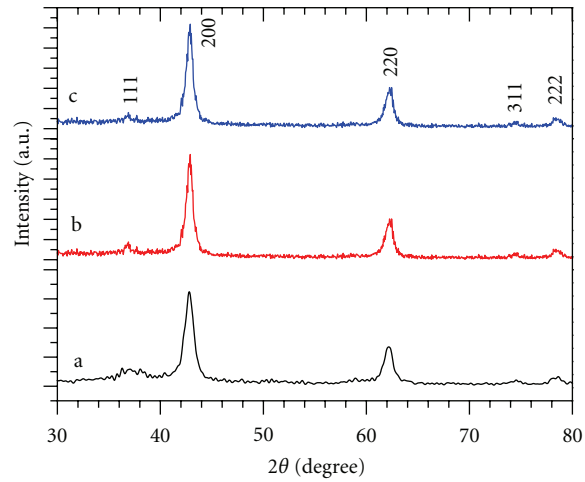


Figure 3: XRD patterns of $Mg_{1-x}Ni_xO$ nanopowders formed by decomposition of respective oxalates at 600°C for 2 h each for $x$ equal to (a) 0.01, (b) 0.05, and (c) 0.10 indicating formation of f.c.c. (NaCl-type) phase similar to magnesium oxide.

content ($x$) equal to 0.01. Moreover, the patterns contain no evidence of any secondary phase. The changes in the lattice parameters are marginal and are on expected line as $Ni^{2+}$ ions occupy $Mg^{2+}$ sites in MgO and both the ions have nearly the same size (ionic radii of $Ni^{2+}$ and $Mg^{2+}$ in octahedral configuration being 0.69 and 0.72 Å, resp.). The average grain size has been determined from the Scherrer formula, $D = 0.9\lambda/\beta\cos\theta$ (where $\lambda$ is the wavelength of X-rays and $\beta$ is the full width at half maximum of the diffraction peak at Bragg angle $\theta$), with 200 peak and using silicon as standard to make correction for the instrumental broadening. The values obtained are in the range 11.4–12.6 nm for $Mg_{1-x}Ni_xO$ ($x = 0.01, 0.05$, and 0.10).

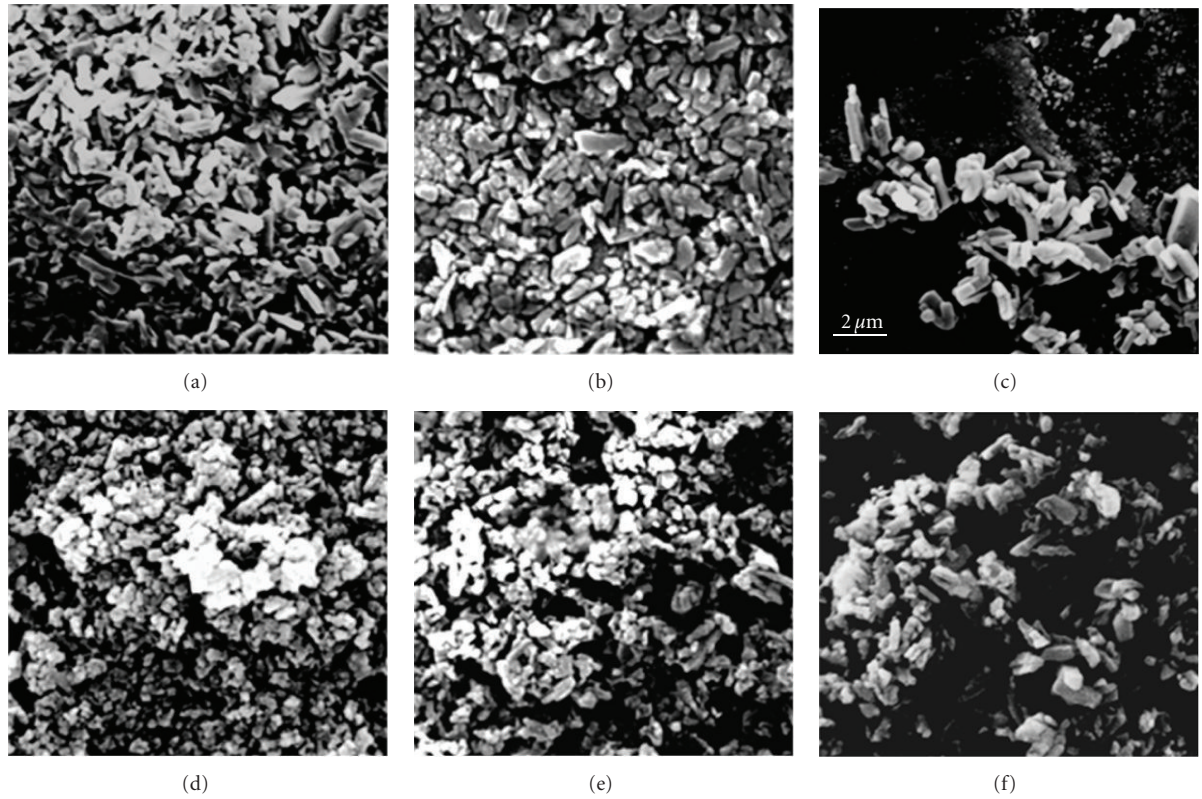


Figure 4: Scanning electron micrographs (a, b, and c) of sol-gel products presumably of oxalates after drying at 100°C for 24 h and (d, e, and f) of corresponding oxide powders, formed by decomposition at 600°C for 2 h each in air for Ni/(Ni+Mg) atomic ratio ($x$) equal to 0.01, 0.05, and 0.10, respectively.

The XRD patterns (not shown here) of $Mg_{1-x}Ni_xO$ ($x$ = 0.01) powder samples obtained by decomposition of sol-gel product in air for 2 h each at 600, 800, and 1000°C reveal slight decrease in the lattice parameter with increase of the decomposition temperature; values being 4.228, 4.223, and 4.212 ± 0.002 Å for 600, 800, and 1000°C, respectively. Clearly, the lattice parameter is approaching the bulk value of MgO and peaks become sharper and stronger with increase in decomposition temperature. This is consistent with previous studies on pure MgO nanopowders [5].

The scanning electron micrographs in secondary electron (SE) mode of magnesium oxalate dihydrate containing different nickel content, that is, [Ni/(Ni+Mg)] atomic ratio ($x$) as 0.01, 0.05, and 0.10, obtained after drying/digesting the sol-gel product at 100°C for 24 h are shown in Figures 4(a), 4(b), and 4(c). These images reveal the emergence of nanorods/nanostrips with varied diameter/width and length in the range 76–120 nm and 312–436 nm, respectively. Also, a few spherical nanoparticles are visible at places independently or within rods. The decomposition of sol-gel products at 600°C for 2 h invariably yields spherical clusters/agglomerates of nanosize particles of nickel doped magnesium oxide (Figures 4(d), 4(e), and 4(f)). Thus, nickel doping in MgO causes little morphological changes in the nature of particles/clusters/agglomerates in comparison to other reports [24, 25].

The values of BET surface area of $Mg_{1-x}Ni_xO$ ($0.01 \leq x \leq 0.10$) powders formed by decomposition of respective oxalates at 600°C for 2 h in air as deduced from nitrogen adsorption isotherms are within 123.0–135.5 $m^2/g$. The corresponding average particle diameter ($d$) has been determined from the formula $d = 6/(s \cdot \rho)$, where s stands for BET specific area and $\rho$ represents the material density (which varies with composition); the values of ($d$) lie in the range 12.0–12.7 nm. These results suggest that nickel doping up to ~10 at% has negligible/no effect on the average particle size. However, the values of ($d$) match reasonably well with the average crystallite size data obtained from XRD for $Mg_{1-x}Ni_xO$ powders. The high BET surface area and small average particle size are expected to improve the characteristics of $Mg_{1-x}Ni_xO$ powders appreciably to make them suitable for applications in plasma display panels [26, 27].

### 3.2. Optical Characteristics

*3.2.1. Infrared Absorption.* The FTIR spectra of sol-gel-derived oxalate samples of Ni/(Ni+Mg) atomic ratios ($x$) 0.01, 0.05, and 0.10 are shown in Figure 5. The broad absorption band around 3408 $cm^{-1}$ is in fact composed of several peaks in the wave number range of 3100–3700 $cm^{-1}$. These correspond to the –OH group stretching vibrations and provide evidence for the presence of chemically bound

Table 1: Optical absorption peaks observed in $Mg_{1-x}Ni_xO$ nanopowders, prepared by decomposition of dried sol-gel-derived oxalate at 600°C for 2 h each in air for nickel content ($x$) = 0, 0.01, 0.05, and 0.10.

| No. | $x$ | Peak 1 | | Peak 2 | | Peak 3 | |
|---|---|---|---|---|---|---|---|
| | | $E$ (eV) | Abs. | $E$ (eV) | Abs. | $E$ (eV) | Abs. |
| 1* | 0 | 6.13[+] | 0.97 | 4.20[#] | 0.20 | 3.27[†] | 0.24 |
| 2 | 0.01 | 6.13 | 0.98 | 4.27 | 0.27 | 3.35 | 0.30 |
| 3 | 0.05 | 6.20 | 1.15 | 4.33 | 0.36 | 3.22 | 0.33 |
| 4 | 0.10 | 6.10 | 1.09 | 4.26 | 0.45 | 3.09 | 0.37 |

* [5].
+ $^1A_{1g} \rightarrow {}^1T_{1u}$ ($1s \rightarrow 2p_x$, $2p_y$, or $2p_z$).
# $^1A_{1g} \rightarrow {}^1E$ ($1s \rightarrow$, $2p_x$ or $2p_y$).
† $^1A_{1g} \rightarrow {}^1A_{1g}$ ($1s \rightarrow 2p_z$).

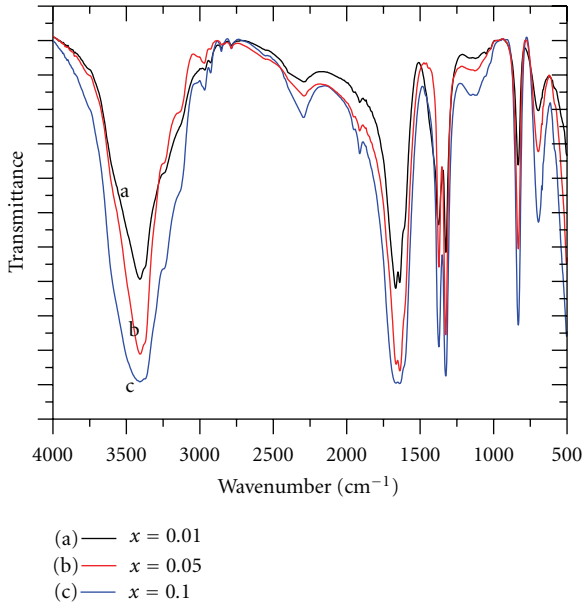


Figure 5: Fourier transform infrared (FTIR) spectra of sol-gel products, each dried at 100°C for 24 h in air, with Ni/(Ni+Mg) atomic ratio equal to (a) 0.01, (b) 0.05, and (c) 0.10.

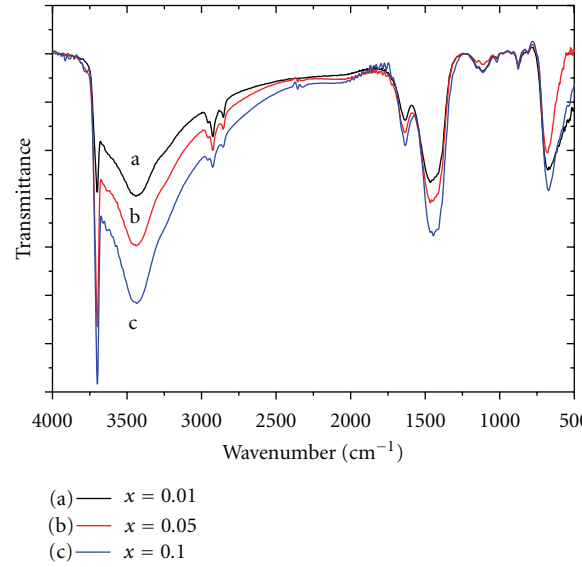


Figure 6: Fourier transform infrared (FTIR) spectra of $Mg_{1-x}Ni_xO$ powders, obtained by decomposition of respective oxalates at 600°C for 2 h each in air for $x$ equal to (a) 0.01, (b) 0.05, and (c) 0.10.

water. The deformational mode of water usually seen around 1650 cm$^{-1}$ is, however, masked by the doublet at 1667 cm$^{-1}$. The other sharp absorption peaks at 1373 and 1325 cm$^{-1}$ are assigned to $\nu_s$ (C–O) and $\delta$ (OC=O) modes. While weak band at 696 cm$^{-1}$ is attributed to bending mode of O=C=O and/or liberation of water, a peak at 501 cm$^{-1}$ is assigned to $\nu$ (Mg–O) + $\nu$ (C–C) modes [5, 28, 29].

Figure 6 shows the FTIR transmittance spectra of $Mg_{1-x}Ni_xO$ ($x$ = 0.01, 0.05, and 0.10) produced by decomposition of Ni-doped $\alpha$-$MgC_2O_4 \cdot 2H_2O$ at 600°C for 2 h in air. These contain signatures of adsorption and chemisorption of water. The sharp peak centred around 3699 cm$^{-1}$ indicates the presence of hydroxyl group at the low-coordination sites or defects [5, 28, 29]. The absorption band in the wave number range 3672–3000 cm$^{-1}$ is quite broad and can be assigned to –OH-stretching mode of adsorbed $H_2O$ on the surface of oxide crystallites. The absorption band in the range of 1300–1750 cm$^{-1}$ is related to hydroxyl groups of molecular water. Since the spectra were not recorded in situ, the products could reabsorb some water from the ambient.

*3.2.2. UV-VIS Absorption.* The optical absorption spectra of $Mg_{1-x}Ni_xO$ ($x$ = 0.01, 0.5, 0.1) powders, obtained by decomposition of dried sol-gel product at 600°C for 2 h in air, in the wavelength range of 200–800 nm are shown in Figure 7. The optical absorption of pure MgO prepared similarly has already been presented elsewhere [5]. Table 1 summarises the optical data in terms of peak energy and absorbance. In pure MgO, a magnesium atom donates two electrons from its $3s^2$-orbitals to 2p-orbitals of oxygen. An energy band gap is thus created between the valence band (oxygen 2p) and conduction band (magnesium, 3s). The known value of energy band gap ($E_g$) of MgO is about 7.8 eV [5, 27]. A strong absorption band near 202 nm and two other peaks around 296 and 379 nm appear in pure MgO. The former corresponds to ($^1A_{1g} \rightarrow {}^1T_{1u}$) transition from $^3P_2$ state

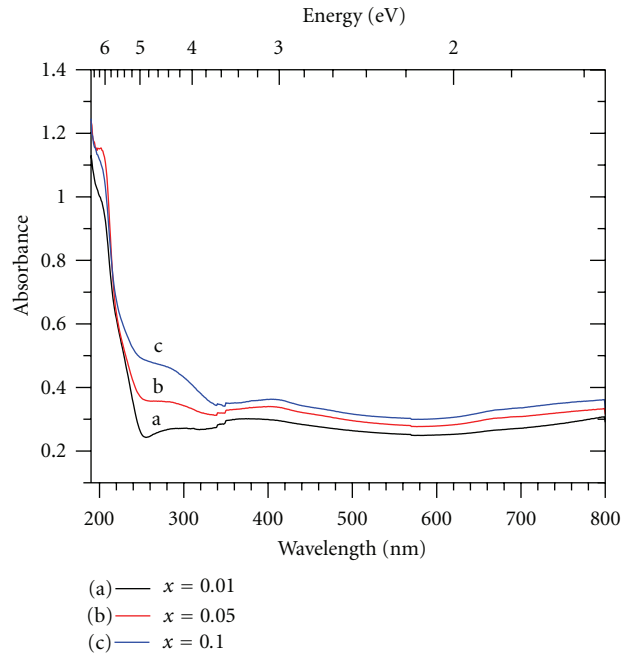


Figure 7: Optical absorption spectra of $Mg_{1-x}Ni_xO$ powders, obtained by decomposition of respective oxalates at 600°C for 2 h each in air for $x$ equal to (a) 0.01, (b) 0.05, and (c) 0.10.

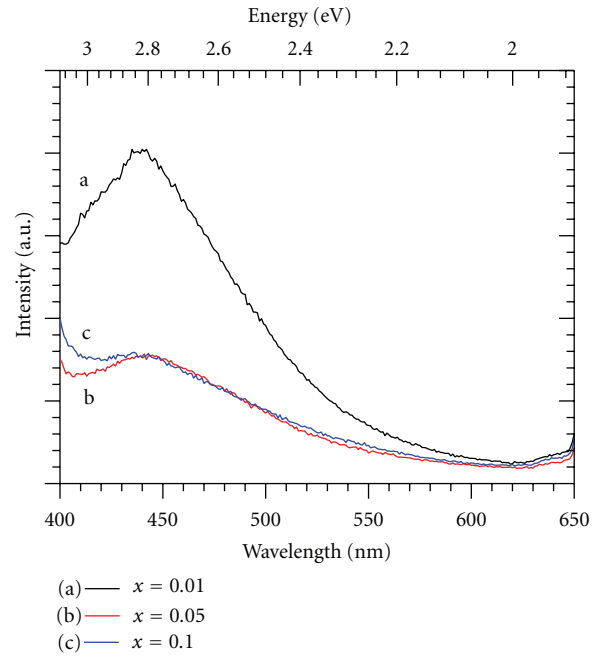


Figure 8: Photoluminescence (PL) spectra of the $Mg_{1-x}Ni_xO$ powders for $x$ equal to (a) 0.01, (b) 0.05, and (c) 0.10.

of oxygen ($O^{2-}$) to $^1S_0$ state of magnesium ($Mg^{2+}$). The other two peaks at 296 and 379 nm are assigned to $^1A_{1g} \rightarrow {}^1E$ ($1s \rightarrow 2p_x$ or $2p_y$) and $^1A_{1g} \rightarrow {}^1A_{1g}$ ($1s \rightarrow 2p_z$) transitions of oxygen defect centres [5, 30]. With incorporation of $Ni^{2+}$ ions in MgO, absorption peaks shift slightly, and correspond to improved absorbance (Table 1, Figure 7). Since no additional band appears, $Ni^{2+}$ ion is possibly substituting $Mg^{2+}$ ion in MgO but somehow influencing the absorbance significantly.

*3.2.3. Photoluminescence (PL) Behaviour.* Photoluminescence (PL) spectra of $Mg_{1-x}Ni_xO$ ($x = 0.01, 0.05, 0.10$) powders, obtained by decomposition of respective oxalates at 1000°C for 2 h in air, with the excitation wavelength of 350 nm are shown in Figure 8. They exhibit a luminescence band centred at 440 nm which becomes broad and shifts slightly towards a higher wavelength (or lower energy) when Ni content ($x$) increases in MgO matrix. Further, a new emission peak begins to develop near 400 nm and its intensity increases progressively with nickel concentration. This observation suggests changes in the symmetry and vibrational modes around the luminescent centres with nickel doping. Since there is small difference and ionic radius of $Ni^{2+}$ (0.69 Å) being smaller than $Mg^{2+}$ (0.72 Å), the former is possibly substituting the latter in MgO.

Pure MgO sample prepared similarly exhibits two emission peaks (strong around 440 nm and weak at 395 nm) with the excitation wavelength of 350 nm and are assigned to $^2B_{1u} \rightarrow {}^1A_g$ and $^2T_{1u} \rightarrow {}^2A_{1g}$ transitions, respectively [8]. Moreover, their origin lies with the existence of $F_2{}^{2+}$ (or $F^+$ dimers) and $F^+$-colour centres, respectively, $F^+$ being oxygen vacancy retaining one electron [8]. This fact in conjunction with the above results indicates that partial substitution of $Mg^{2+}$ by $Ni^{2+}$ ions causes decrease of $F^+$ dimers with simultaneous increase of $F^+$-defect centres in MgO. The process can occur in two ways, namely, $F^+$ dimer either splits into two $F^+$ centres or converts into one $F^+$ centre with transfer of extra electron rendering $Ni^{2+} \rightarrow Ni^{1+}$conversion. It may be mentioned that $Ni^{2+}$ ion has an empty ($e_g$) low-spin orbital.

Photoluminescence studies of pure MgO nanocrystals with excitation wavelength of 273 nm have revealed a broad emission band centred around 350 nm arising due to oxygen vacancies [13, 30]. In $Dy^{3+}$-doped MgO, emission peaks appear at 480 nm and 575 nm due to $^4F_{9/2}-{}^6H_{15/2}$ and $^4F_{9/2}-{}^6H_{13/2}$ transitions of dysprosium [18]. In fact, $Dy^{3+}$-ions encounter difficulty in substitution because of their large size (ionic radii being 0.91 Å against 0.72 Å of $Mg^2$) and therefore lie essentially on the surface or in the grain boundaries giving its own PL emission at 575 nm. On the other hand, $Ni^{2+}$ ions can assume $Mg^{2+}$ sites easily and influence the nature of emission. As a consequence, the peak at 440 nm diminishes and that near 400 nm rises due to decrease in $F_2{}^{2+}$ centres (or dimers) and formation of additional $F^+$ centres occurring in MgO.

Upon substitution, $Ni^{2+}$ ion occupies an octahedral void in MgO and so is coordinated with six oxygen ions. The energy level diagram of $Ni^{2+}$ ($3d^8$) ion suggests three major thermoradiative energy transitions, $^1A_1 \rightarrow {}^1E$ (1117 nm, 1.110 eV), $^3T_2 \rightarrow {}^3A_2$ (1256 nm, 0.987 eV), and $^1T_2 \rightarrow {}^1E$ (1414 nm, 0.877 eV) at 1300–1400°C. Thus, Ni-doped MgO may also serve as a potential emitter for thermophotovoltaic

(TPV) generators [20, 21]. Work is in progress in this direction.

## 4. Conclusions

$Mg_{1-x}Ni_xO$ nanopowders synthesized by decomposition of sol-gel-derived oxalate in air at 600°C or above for 2 h exhibit (i) an f.c.c. (NaCl-type) structure with a typical lattice parameter of 4.228(2) Å at $x = 0.01$, (ii) three optical absorption bands at 6.13 eV, 4.27 eV, and 3.35 eV corresponding to $^1A_{1g} \rightarrow {}^1T_{1u}$, $^1A_{1g} \rightarrow {}^1E$, and $^1A_{1g} \rightarrow {}^1A_{1g}$ transitions, and (iii) signature of water affinity with a sharp peak at 3699 $cm^{-1}$ and bands in the range 3672–3000 $cm^{-1}$ and 1300–1750 $cm^{-1}$ in the FTIR spectra. Their photoluminescence characteristics with the excitation wavelength of 350 nm depend on the nickel content and are altered in terms of emission (i) reduction at 440 nm due to decrease in $F_2{}^{2+}$ centres and (ii) enhancement near 400 nm because of emergence of additional $F^+$ centres. Ni-doped MgO may serve as emitter in thermophotovoltaic generators too.

## References


[1] R. Riedel and I.-W. Chen, *Ceramics Science and Technology: Materials and Properties*, vol. 2, Wiley-VCH, Weinheim, Germany, 2010.

[2] N. A. Vasil'eva and N. F. Uvarov, "Electrical conductivity of magnesium oxide as a catalyst for radical chain hydrocarbon pyrolysis reactions," *Kinetics and Catalysis*, vol. 52, no. 1, pp. 98–103, 2011.

[3] S. A. El-Molla, S. M. Abdel-all, and M. M. Ibrahim, "Influence of precursor of MgO and preparation conditions on the catalytic dehydrogenation of iso-propanol over CuO/MgO catalysts," *Journal of Alloys and Compounds*, vol. 484, no. 1-2, pp. 280–285, 2009.

[4] M. A. Shah and F. M. Al-Marzouki, "Bio-safe approach for the preparation of magnesium oxide (MgO) nanoflowers at very low temperature," *International Journal of Biomedical Nanoscience and Nanotechnology*, vol. 1, pp. 10–16, 2010.

[5] A. Kumar and J. Kumar, "On the synthesis and optical absorption studies of nano-size magnesium oxide powder," *Journal of Physics and Chemistry of Solids*, vol. 69, no. 11, pp. 2764–2772, 2008.

[6] A. A. Yar, M. Montazerian, H. Abdizadeh, and H. R. Baharvandi, "Microstructure and mechanical properties of aluminum alloy matrix composite reinforced with nano-particle MgO," *Journal of Alloys and Compounds*, vol. 484, no. 1-2, pp. 400–404, 2009.

[7] S. H. Tamboli, V. Puri, and R. K. Puri, "Improvement in adhesion and decrease in stress of MgO thin films due to vapour chopping," *Journal of Alloys and Compounds*, vol. 503, no. 1, pp. 224–227, 2010.

[8] A. Kumar, S. Thota, S. Varma, and J. Kumar, "Sol-gel synthesis of highly luminescent magnesium oxide nanocrystallites," *Journal of Luminescence*, vol. 131, no. 4, pp. 640–648, 2011.

[9] J.-S. Choi, S.-H. Moon, J.-H. Kim, and G.-H. Kim, "The effects of high purity MgO nano-powders on the electrical properties of AC-PDPs," *Current Applied Physics*, vol. 10, no. 6, pp. 1378–1382, 2010.

[10] A. M. E. Raj, T. Som, V. Ganesan et al., "Tailoring optical and electrical properties of MgO thin films by 1.5 MeV $H^+$ implantation to fluences," *Nuclear Instruments and Methods in Physics Research B*, vol. 266, no. 11, pp. 2564–2571, 2008.

[11] L. A. Ma, Z. X. Lin, J. Y. Lin, Y. A. Zhang, L. Q. Hu, and T. L. Guo, "Large-scale growth of ultrathin MgO nanowires and evaluate their field emission properties," *Physica E*, vol. 41, no. 8, pp. 1500–1503, 2009.

[12] J. H. Zhang, X. L. Zhou, and J. A. Wang, "Water promotion or inhibition effect on isopropanol decomposition catalyzed with a sol-gel MgO-$Al_2O_3$ catalyst," *Journal of Molecular Catalysis A*, vol. 247, no. 1-2, pp. 222–226, 2006.

[13] F. Gu, C. Li, H. Cao et al., "Crystallinity of Li-doped MgO:$Dy^{3+}$ nanocrystals via combustion process and their photoluminescence properties," *Journal of Alloys and Compounds*, vol. 453, no. 1-2, pp. 361–365, 2008.

[14] L.-Z. Peia, L.-Z. Yinb, J.-F. Wanga, J. Chena, C.-G. Fana, and Q.-F. Zhanga, "Low temperature synthesis of magnesium oxide and spinel powders by a sol-gel process," *Materials Research*, vol. 13, no. 3, pp. 339–343, 2010.

[15] M. Nusheh, H. Yoozbashizadeh, M. Askari, H. Kobatake, and H. Fukuyama, "Mechanically activated synthesis of single crystalline MgO nanostructures," *Journal of Alloys and Compounds*, vol. 506, no. 2, pp. 715–720, 2010.

[16] J. Narayan, S. Nori, D. K. Pandya, D. K. Avasthi, and A. I. Smirnov, "Defect dependent ferromagnetism in MgO doped with Ni and Co," *Applied Physics Letters*, vol. 93, no. 8, Article ID 082507, 2008.

[17] W. Wang, X. Qiao, J. Chen, and F. Tan, "Preparation and characterization of Ti-doped MgO nanopowders by a modified coprecipitation method," *Journal of Alloys and Compounds*, vol. 461, no. 1-2, pp. 542–546, 2008.

[18] F. Gu, S. F. Wang, M. K. Lü et al., "Combustion synthesis and luminescence properties of $Dy^{3+}$-doped MgO nanocrystals," *Journal of Crystal Growth*, vol. 260, no. 3-4, pp. 507–510, 2004.

[19] W. Wang, X. Qiao, J. Chen, F. Tan, and H. Li, "Influence of titanium doping on the structure and morphology of MgO prepared by coprecipitation method," *Materials Characterization*, vol. 60, no. 8, pp. 858–862, 2009.

[20] L. G. Ferguson and F. Dogan, "Spectral analysis of transition metal-doped MgO "matched emitters" for thermophotovoltaic energy conversion," *Journal of Materials Science*, vol. 37, no. 7, pp. 1301–1308, 2002.

[21] S. Basu, Y.-B. Chen, and Z. M. Zhang, "Microscale radiation in thermophotovoltaic devices—a review," *International Journal of Energy Research*, vol. 31, no. 6-7, pp. 689–716, 2007.

[22] A. Kumar and J. Kumar, "Perspective on europium activated fine-grained metal molybdate phosphors for solid state illumination," *Journal of Materials Chemistry*, vol. 21, no. 11, pp. 3788–3795, 2011.

[23] T. Yoshida, T. Tanaka, H. Yoshida, T. Funabiki, and S. Yoshida, "Study on the dispersion of nickel ions in the NiO-MgO system by x-ray absorption fine structure," *Journal of Physical Chemistry*, vol. 100, no. 6, pp. 2302–2309, 1996.

[24] F. Arena, A. L. Chuvilin, and A. Parmaliana, "Characterization of Li-doped Ni/MgO catalysts," *Journal of Physical Chemistry*, vol. 99, no. 3, pp. 990–998, 1995.

[25] S. Bhatia, N. A. Binti Mohd Zabidi, and M. H. A. R. Bin Megat Ahmad, "Catalytic activity and morphological properties of Ni/MgO catalysts for the oxidative coupling of methane," *Reaction Kinetics and Catalysis Letters*, vol. 74, no. 1, pp. 87–92, 2001.

[26] M. H. Lee and D. G. Park, "Preparation of MgO with high surface area, and modification of its pore characteristics," *Bulletin of the Korean Chemical Society*, vol. 24, no. 10, pp. 1437–1443, 2003.

[27] L. Delle Site, A. Alavi, and R. M. Lynden-Bell, "The structure and spectroscopy of monolayers of water on MgO: an ab initio study," *Journal of Chemical Physics*, vol. 113, no. 8, pp. 3344–3350, 2000.
[28] K. Nakamoto, *Infrared Spectra of Inorganic and Coordination Compounds*, John Wiley & Sons, London, UK, 1963.
[29] A. Kumar and J. Kumar, "Defect and adsorbate induced infrared modes in sol-gel derived magnesium oxide nanocrystallites," *Solid State Communications*, vol. 147, no. 9-10, pp. 405–408, 2008.
[30] M. A. Shah and A. Qurashi, "Novel surfactant-free synthesis of MgO nanoflakes," *Journal of Alloys and Compounds*, vol. 482, no. 1-2, pp. 548–551, 2009.